

Robust Time Series Denoising with Learnable Wavelet Packet Transform

Gaëtan Frusque , Olga Fink.

Abstract—In many applications, signal denoising is often the first pre-processing step before any subsequent analysis or learning task. In this paper, we propose to apply a deep learning denoising model inspired by a signal processing, a learnable version of wavelet packet transform. The proposed algorithm has significant learning capabilities with few interpretable parameters and has an intuitive initialisation. We propose a post-learning modification of the parameters to adapt the denoising to different noise levels. We evaluate the performance of the proposed methodology on two case studies and compare it to other state of the art approaches, including wavelet shrinkage denoising, convolutional neural network, autoencoder and U-net deep models. The first case study is based on designed functions that have typically been used to study denoising properties of the algorithms. The second case study is an audio background removal task. We demonstrate how the proposed algorithm relates to the universality of signal processing methods and the learning capabilities of deep learning approaches. In particular, we evaluate the obtained denoising performances on structured noisy signals inside and outside the classes used for training. In addition to having good performance in denoising signals inside and outside to the training class, our method shows to be particularly robust when different noise levels, noise types and artifacts are added.

Index Terms—Denoising, deep learning, wavelet packet transform, time series, acoustic signals

I. INTRODUCTION

Real world signals are often corrupted by noise which needs be removed before any further analysis or processing step. To solve this problem, several contributions based on different approaches have been proposed. Several approaches for signal denoising have been proposed. This includes approaches such as dictionary learning [1], empirical mode decomposition [2], singular and higher order singular values decomposition [3], [4] or canonical polyadic decomposition [5]. [6], reviewed denosing approaches for biomedical signals and [7] for images. Particularly wavelet-based methods are considered as an essential tool for multi-resolution and time-frequency analysis [8]. The wavelet shrinkage operation that was theoretically investigated in [9] is still considered as one of the most powerful tools to perform signal denoising in many fields. Thus, wavelet

packet transform (WPT) denoising has been used recently [10], [11] due to its ability to denoise regular frequency bands of desired size and to remove backgrounds with a specific frequency content.

To perform wavelet denoising, several hyperparameters need to be set. The parameters include the threshold used for wavelet shrinkage, the thresholding function and the wavelet family considered for the decomposition. Several heuristics have been proposed to address threshold selection [12], such as the universal threshold [9], Stein's unbiased risk estimation or the Bayesian shrink method [13]. However, the selection of the wavelet family and the correct heuristics require specialized knowledge to remain robust to the complexity of the real data. Recent work opts for learning or automating the best hyperparameter configuration by supervised learning from a training dataset. In [12] a genetic algorithm is used to find the best wavelet denoising strategy for EEG denoising. These methods benefit from the recent evolution of storage capacities and computing power allowing the constant increase of the amount of data collected to form the training dataset.

For supervised denoising, deep learning methods have recently made a significant progress, particularly in application areas with large amounts of data, such as image denoising [14] or speech enhancement [15]. The use of deep neural networks (NNs) for denoising in domains where data is more specific and difficult to collect, such as biological signals, is a current issue [6], [16]. The main supervised denoising architectures based on deep learning include the convolutional neural network (CNN) [17] Convolutional Auto-Encoder (AE) [18] and the U-Net [19].

Recently, deep architectures inspired by signal processing approaches have been proposed [20]. The main advantages of these approaches are to find more meaningful CNN filters, to gain in interpretability and to reduce the number of parameters [21]. In this work, we propose to combine two of the main signal denoising methodologies, namely WPT denoising with wavelet shrinkage and deep autoencoder denoising. Thus, we use a WPT-based deep learning architecture with learnable activation functions mimicking wavelet shrinkage, referred to as Learnable WPT (L-WPT). The proposed method is a relaxed version of the L-WPT architecture of [22] to improve learning capabilities. This is the first application of L-WPT for a denoising task. The advantage of this architecture is threefold: a) It is based on a very powerful signal processing approach to obtain a time-frequency representation with optimal resolution. This provides our L-WPT algorithm considerable learning capabilities with only few parameters

Manuscript submitted May 28, 2019. This study was supported by the Swiss Innovation Agency (Innosuisse) under grant number: 47231.1 IP-ENG.

G. Frusque and O. Fink are with Laboratory of Intelligent Maintenance and Operations Systems, EPFL, Lausanne, gaetan.frusque@epfl.ch, olga.fink@epfl.ch

compared to standard deep learning methods [23], [22].
b) The L-WPT contains only interpretable parameters that can be adapted manually if the operating conditions change.
c) We propose an intuitive initialization of the parameters to make the behaviour of the L-WPT as close as possible to the standard WPT.

As a second contribution, we demonstrate in this work how our L-WPT is related to the universality of signal processing methods and the learning capabilities of deep learning approaches. This highlights the advantage of combining signal processing and deep learning methods. Specifically, we evaluate on the one hand how well the L-WPT can specialize and learn the particularity of the training dataset, and on the other hand how well it is able to generalize to information and artifacts that are different to the one contained in the training data.

After presenting the related work in Section II, we provide the necessary background on WPT in Section III. The proposed L-WPT for signal denoising is introduced in Section IV. A comparative study between the proposed L-WPT and several deep NNs is made using a standard model for signal denoising in Section P3. Finally, the performance of the L-WPT is highlighted in the real case of background removal in Section refSection4 before concluding.

II. RELATED WORK

Wavelet denoising: Wavelet shrinkage consists, after the application of a wavelet transform, in removing the low amplitude coefficients associated with noise. Different type of wavelet transform have been proposed. It can be any orthogonal wavelet transform [8], or iterative methods such as the discrete wavelet transform (DWT). The latter provides a representation of a signal in frequency bands of different temporal resolution. DWT has been applied among others for biomedical signals [12], [11], speech signals [24], [25], and partial discharge applications [10]. Unlike DWT, Wavelet Packet Transform (WPT) has the advantage of denoising on frequency bands of the same width. WPT denoising has been applied in various fields including speech enhancement [26], [27], noise detection in bio-signals [28] and atomic force microscopy image denoising [29]. WPT has proven to be particularly suitable for background denoising with a specific frequency content. However the settings of the thresholds for each frequency band is a challenging task [30], [31].

Deep-learning-based supervised denoising: The multilayer perceptron can be considered as the most basic deep neural network architecture. In the context of speech enhancement, this architecture has proven to be less robust and more difficult to train due to its high number of parameters compared to other methods such as the convolutional neural networks (CNNs) [19], [32]. The CNN uses the convolution operation. Only local and sparse connections between the input and output of each layers are considered. This reduces the number of parameters considerably and facilitates the learning process. CNN-based denoising methods have been used in several applications such as ECG denoising [16], speech enhancement

[17] or image denoising [14]. In [33], a CNN is used to separate sound events from the background in the time-frequency domain to improve sound classification. The auto-encoder version of the CNN, the convolutional auto-encoder (AE) has been one the most widely used architectures for denoising. AE aims to produce an input-like representation using an encoder and a decoder. The objective of the encoder is to find an embedding of the input data that contains the important information, eliminating noise. A noise-free signal based on the embedding is estimated with the decoder [34]. Several examples of AE-based denoising methods can be found in the literature. For example, in [18], an autoencoder is used to denoise the vibration signals from the bearing dataset. The denoising step helps in monitoring the condition of the bearing by improving fault diagnosis. As another example, a blind denoising autoencoder was used for image processing [35] where only noisy samples are used for the training. One challenge encountered by AE is the potential loss of important information with the increasing number of layers. Adding skip connections to create a U-Net architecture [36] can potentially tackle this problem. As shown in the comparative study in [19], the U-Net architecture as proposed in [37] has the best overall performance compared to several other architectures without skipped connections. Several recent works on image denoising also demonstrate a good performance of U-Net denoising [38].

Deep NNs architectures inspired by signal processing: Several approaches that include signal processing elements in NNs have already been proposed. In [20], a CNN layer with kernels constrained to match bandpass filters only are used for speaker recognition. In [39] and [40], a deep model simulating a filter bank is used for sound classification and in the field of cosmology. The first learnable extensions of WPT are focused on learning the best filter to use in through the entire architecture, such as in [41], [42], [43], [40]. The authors in [23] proposed the DeSpaWN model. It is the first model to generalize filter learning to each layer and to add activation functions that perform automatic denoising in the context of DWT. DeSpaWN has been successfully applied to classification and anomaly detection tasks for audio signals. An extension of the DeSpaWN architecture to WPT, called L-WPT, was proposed in [22]. The L-WPT shows a better performance compared to DeSpaWN for the same anomaly detection task. The proposed method is an extension of the L-WPT architecture from [22] that is free of WPT constraints.

III. BACKGROUND

A. Wavelet Packet Transform (WPT)

The discrete WPT, introduced in [44], projects the signal on uniform frequency bands of desired size. The WPT has a multi-level structure and can be considered as a multi-resolution analysis since the output of the current level is recursively used as input to the next level. The basic bloc of a WPT applied to an input signal \mathbf{y} is:

$$(\mathbf{y}^{lp})_{(n)} = (\mathbf{h}^{lp} * \mathbf{y})_{(2n)}, \quad (\mathbf{y}^{hp})_{(n)} = (\mathbf{h}^{hp} * \mathbf{y})_{(2n)}, \quad (1)$$

where $*$ is the convolution operation and \mathbf{y}^{lp} (or \mathbf{y}^{hp}) corresponds to the low- (or high-) pass filtered input data with a cut-off frequency of $\pi/2$ followed by a sub-sampling by two. This transformation doubles the frequency resolution (the frequency content of each wavelet coefficient spans half the input data frequency) to the detriment of a halved time resolution (\mathbf{y}^{lp} and \mathbf{y}^{hp} each contains half the number of samples in \mathbf{y}). By applying the same block Eq. (1) on \mathbf{y}^{lp} and \mathbf{y}^{hp} , we then obtain four outputs that divide the frequency content of the input signal in four even bands. As shown in Figure 1, the underlying algorithm behind of WPT has a tree structure characterised by L layers, corresponding to the number of times we apply the block Eq. (1) to the outputs of the previous layer. We refer to the nodes as the succession of a filtering and a sub-sampling operation. The outputs from the 2^L nodes at layer L form the time-frequency representation of our signal \mathbf{y} .

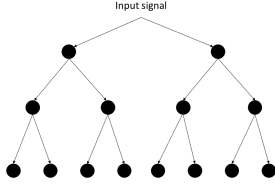


Fig. 1: Tree structure of the WPT algorithm. Each node corresponds to the succession of a filtering and a sub-sampling operation.

B. Perfect reconstruction

It is possible to recover the input signal \mathbf{y} from \mathbf{y}^{lp} and \mathbf{y}^{hp} thanks to the following operation:

$$\mathbf{y} = \mathbf{h}^{T-lp} * \text{up}[\mathbf{y}^{lp}] + \mathbf{h}^{T-hp} * \text{up}[\mathbf{y}^{hp}], \quad (2)$$

where the up-sampling operation $\text{up}[\bullet]$ is necessary to counteract the effect of the down-sampling in Eq. (1). It can be defined as $\text{up}[\mathbf{x}]_{(2n)} = x_{(n)}$ and $\text{up}[\mathbf{x}]_{(2n+1)} = 0$. To ensure a perfect reconstruction, the kernels of the filters \mathbf{h}^{lp} , \mathbf{h}^{T-lp} , \mathbf{h}^{hp} and \mathbf{h}^{T-hp} have to respect the following properties [45]:

- \mathbf{h}^{hp} has to be the Alternating Flip (AF) of \mathbf{h}^{lp} . It causes both filters to have mirrored magnitude responses around $\pi/2$. The AF of a filter \mathbf{h} is denoted as $\text{flip}[\mathbf{h}]$ and corresponds, for a filter of size $K+1$ with K an odd number and $k \in \{0, \dots, K\}$, to:

$$\text{flip}[\mathbf{h}]_{(k)} = (-1)^k (\mathbf{h})_{(K-k)}. \quad (3)$$

- the transposed filters \mathbf{h}^{T-lp} and \mathbf{h}^{T-hp} have to be defined as the delayed paraconjugate of \mathbf{h}^{hp} and \mathbf{h}^{lp} . By doing so, the Anti-Cancellation Conditions (ACC) will be respected and the aliasing terms due to the use of non-ideal filters will be removed. The delayed paraconjugate of the real filter \mathbf{h} results in $\bar{\mathbf{h}}$ with:

$$(\bar{\mathbf{h}})_{(k)} = (\mathbf{h})_{(K-k)}. \quad (4)$$

- by respecting the AF and ACC properties, the kernels of the filters \mathbf{h}^{T-lp} , \mathbf{h}^{hp} and \mathbf{h}^{T-hp} become a function of the kernel of the filter \mathbf{h}^{lp} . One additional property is then necessary to ensure the conservation of the frequency content through the tree structure: the \mathbf{h}^{lp} kernel has to be normalised and double-shift orthogonal (for non-null shifts). Then, \mathbf{h}^{hp} and \mathbf{h}^{lp} will be conjugate mirrors [46] and the power sum of both filters will be one for all frequencies.

With these properties, it becomes easy to demonstrate that a perfect reconstruction of the WPT of a signal from any layer L is possible. This operation is called inverse WPT (iWPT).

C. Denoising with WPT

Signal denoising is one of the major applications of wavelet analysis [8]. It has been shown that, a wavelet transform will lead to a sparse decomposition of regular and structured signals [46]. We can then assume that the noise will correspond to wavelet coefficients of small amplitudes. Several procedures eliminating small coefficients of a WPT already exists [8], [9]. The two most commonly applied approaches use the soft- and hard-thresholding operators [9]. The soft-thresholding appears to be more adequate for image denoising with small signal-to-noise ratios (SNR). We propose in this paper to study only the hard thresholding (HT) operation to eliminate the low coefficients of the WPT. Considering a WPT with L layers, and $y_L^i(t)$ one of the obtained coefficients at node i , the HT operation with threshold value λ corresponds to:

$$HT_\lambda(y_L^i(t)) = \begin{cases} y_L^i(t) & \text{if } |y_L^i(t)| > \lambda, \\ 0 & \text{else} \end{cases} \quad (5)$$

The operation has to be performed for all coefficients with index t , and all nodes i of the layer L . An estimation of the denoised input signal can then be computed by applying the iWPT to the thresholded coefficients.

For a better understanding, we propose to evaluate the impact of the HT denoising strategy on cosines of different frequencies and amplitudes. The frequency range goes from 0 Hz to the maximum frequency (2^{*12} Hz), and the amplitude range goes from 0 to 1.5. Figure 2 shows the gain score, which is the ratio of the norm of the input signal and the norm of the output signal, in function of the amplitude and the frequency of the input cosine. When cosines have a too low amplitude, they are interpreted as noise and are not reconstructed, which corresponds to a gain score of 0. On the contrary, cosines with a high amplitude are perfectly reconstructed and have a score of 1. The frequency has no impact because the same threshold is used for each node of the WPT. Some imperfections are present since the applied filters are not ideal.

IV. LEARNABLE WAVELET PACKET TRANSFORM

The proposed method is a modification of the recently proposed learnable deep architecture, Learned-WPT (L-WPT), [22]. This section details the proposed methodology.

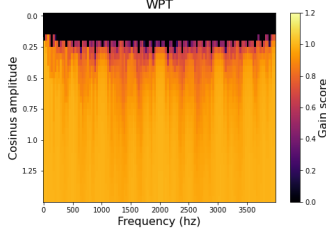


Fig. 2: Gain score from pure cosine signal with increasing frequencies and amplitudes for the WPT with HT denoising considering a thresholding value $\lambda = 1$.

A. Adapted denoising

As shown in Figure 2, one of the major problems of the HT denoising method presented in Section III-C is that it does not adapt to the frequency of the input signal. This can be problematic if the background noise we want to remove from the pure signal has a structured frequency content. Some methodologies adapting the thresholding value according to the frequency have been previously proposed [30], [31], [12]. We propose to go further by applying an adapted activation function with learnable biases to each node of the entire tree structure of the WPT algorithm. The proposed activation function will perform a learnable thresholding eliminating the coefficients related to noise.

In order to have a differentiable thresholding function, we propose the double sharp sigmoid activation function proposed in [23] and denoted as $\eta_\gamma(x)$:

$$\eta_\gamma(x) = x \left[\frac{1}{1 + e^{10(x+\gamma)}} + \frac{1}{1 + e^{-10(x-\gamma)}} \right], \quad (6)$$

with γ the learned bias acting as a threshold on both sides of the origin.

B. L-WPT: an autoencoder model inspired by WPT

The proposed L-WPT methodology is an instance of autoencoders, where the encoding part mimics the tree structure algorithm of the WPT and the decoding part mimics the inverse tree structure of the iWPT. Since the WPT will provide a sparse representation only for structured signals respecting specific properties [46] which does not always hold for real applications, we propose to learn the WPT filters. The idea is to find an adapted sparse representation of the signal of interest, which, combined with the proposed denoising activation function Eq. 6, will be able to better convert a potentially complex noise into low coefficients that can be then eliminated.

Thus, considering the encoding part, the filter used in each node is replaced by a convolutional layer with the stride two followed by the denoising activation function Eq. 6. To obtain the coefficients at layer l and node i (denoted \mathbf{y}_l^i), we need to convolve the coefficients at the previous layer with the kernel of the current node, denoted

by θ_l^i , and apply the activation function Eq. 6. It can be written as:

$$\mathbf{y}_l^i = \eta_{\gamma_l^i} \left(\theta_l^i * \mathbf{y}_{l-1}^{\lfloor \frac{i}{2} \rfloor} \right), \quad (7)$$

where $\lfloor \bullet \rfloor$ corresponds to floor function. The activation function is applied at each coefficient of \mathbf{y}_l^i with the learnable bias value γ_l^i . An illustration providing an comparison of the operations performed in a WPT node and a L-WPT node is shown in Figure 3

For the decoding part, we only replace the filters by a transposed convolutional layer with stride 2. It is possible to compute a denoised estimation of the coefficients at layer l and node i (denoted $\hat{\mathbf{y}}_l^i$) by using the denoised estimation of the higher layers and two kernels denoted as β_{l+1}^{2i} and β_{l+1}^{2i+1} . It can be formulated as:

$$\hat{\mathbf{y}}_l^i = \beta_{l+1}^{2i} * \text{up}[\hat{\mathbf{y}}_{l+1}^{2i}] + \beta_{l+1}^{2i+1} * \text{up}[\hat{\mathbf{y}}_{l+1}^{2i+1}] \quad (8)$$

Considering these notations, the input signal can be denoted as \mathbf{y}_0^0 , the output signal as $\hat{\mathbf{y}}_L^0$ and we have $\mathbf{y}_L^i = \hat{\mathbf{y}}_L^i \forall i \in \{0, \dots, 2^L - 1\}$.

In the previous work [22], [23], the ACC and AF constraints presented in Section III-B are added to the architecture. This has the advantage of limiting the number of coefficient in the L-WPT, and make the approach closer to the standard WPT. We propose for this application, to maximise the learning capabilities of the L-WPT by being free of those two constraints.

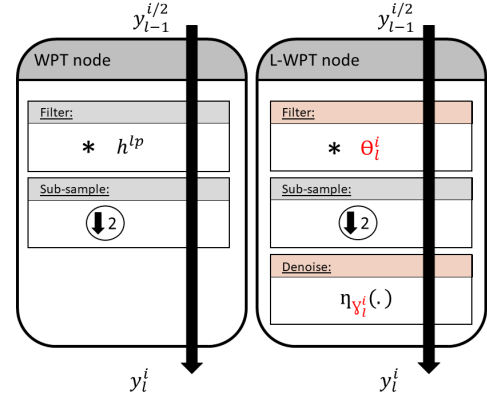


Fig. 3: Comparison between the operations performed in the WPT node (left) and a L-WPT node (right). The variables in red are learnable. If we consider a WPT node using the \mathbf{h}^{lp} filter the input signal becomes $\mathbf{y}_{l-1}^{(i-1)/2}$.

C. Adaptable weights

Since our architecture is inspired by a signal processing methodology, we have a good understanding of the purpose of each part of the network, and how a modification of the parameters impacts the output signal. The bias of the activation function is meaningful and is used to threshold low amplitude coefficients associated with noise. After learning the kernels and bias, the L-WPT can be applied to denoise signals under different operating conditions and

noise levels. Thus, it is always possible to modify the biases afterwards if, for example, the noise level increases or decreases.

We propose a simple modification of the biases, called δ modification. A trained L-WPT with the δ modification is then denoted as L-WPT-(δ). This modification consists simply in multiplying each bias value by δ and can be written as:

$$\begin{aligned} \gamma_l^i &\leftarrow \delta \gamma_l^i & \forall l \in \{1, \dots, L\} \\ & & \forall i \in \{0, \dots, 2^L - 1\} \end{aligned} \quad (9)$$

δ is chosen according to the variations of the noise level with respect to the training data (see background suppression application section VI-C).

D. Intuitive weight initialisation

One of the advantages of the proposed method is that there are intuitive initializations of filters and biases in order to start with a L-WPT that behaves in a similar way as a standard WPT. Considering a kernel, denoted as \mathbf{h}^{PR} , which satisfies the conjugate mirror property (examples of such kernels include wavelet families like Daubechies, Haar or Coiflets [46]), the initialisation of the kernels in the encoding and decoding parts for all layers l and nodes i is:

$$\theta_l^i = \mathbf{h}^{\text{PR}} \quad \text{if } i \text{ is even,} \quad (10)$$

$$\theta_l^i = \text{flip}[\mathbf{h}^{\text{PR}}] \quad \text{if } i \text{ is odd,} \quad (11)$$

$$\beta_l^i = \bar{\mathbf{h}}^{\text{PR}} \quad \text{if } i \text{ is even,} \quad (12)$$

$$\beta_l^i = \text{flip}[\bar{\mathbf{h}}^{\text{PR}}] \quad \text{if } i \text{ is odd.} \quad (13)$$

The alternating flip ($\text{flip}[\bullet]$) and paraconjugate ($\bar{\bullet}$) are explained section III-B. Thus, the kernel through the L-WPT structure will respect the AF and ACC conditions.

Finally, the denoising activation function has to be replaced by a linear function, which can be done if we initialise all biases γ_l^i with 0.

E. Objective function and training

We denote by s a pure signal, and $\tilde{s} = s + b$ the same signal corrupted by a background noise b . Thus, assuming that we have a set of pure signals and background noise, we are looking for the best kernels of the encoding part $\Theta = [\theta_0^0, \theta_1^0, \theta_1^1, \dots, \theta_L^{2^L-1}]$, kernels of the decoding part $B = [\beta_0^0, \beta_1^0, \beta_1^1, \dots, \beta_L^{2^L-1}]$ and biases $\Gamma = [\gamma_1^0, \gamma_1^1, \dots, \gamma_L^{2^L-1}]$ minimising the following loss function:

$$\underset{\Theta, B, \Gamma}{\text{argmin}} \quad \sum_n \|\hat{s}_n - s_n\|_F^2, \quad (14)$$

where $\hat{s} = \hat{\mathbf{y}}_0^0$ is the reconstructed signal from the input data $\tilde{s} = \mathbf{y}_0^0$.

We use the Adam optimiser [47] with a learning rate of 0.0005 and a batch size of 8 to train the L-WPT. The number of epochs is set to 500 and the learning rate is divided by 10 after the epoch 350 and the epoch 450 for a better convergence. We initialise the filters and bias

as presented in Section IV-D using for \mathbf{h}^{PR} Daubechies wavelet with 8 coefficients (called db4).

By referring to n_p as the number of trainable parameters and considering L layers and $K+1$ coefficients per filters, we have for the L-WPT $n_p = \sum_{l=1}^L 2^L K + \sum_{l=1}^L 2^L$ trainable parameters, where the first part are the filter parameters and the second the biases parameters.

V. DENOISING PERFORMANCES ON STANDARD FUNCTIONS

We compare the L-WPT performance to other deep NNs architectures and wavelet shrinkage for denoising purpose. More details about these methods are given in sub-section V-A. For a benchmark study, we consider standard function classes commonly applied in denoising literature to evaluate the performance of denoising algorithms [9], [48], [2]. They mimic spatially variable functions arising in imaging, spectroscopy and other applications and are presented in sub-section V-B. We demonstrate in sub-section V-C how the training of the L-WPT leads to significant behavior changes compared to WPT with wavelet shrinkage. Then, we quantify in sub-section V-D how this behavior change leads to improve the denoising of signals from the training class, but also signals of different nature from other classes. It will demonstrate how L-WPT relates to the learning capabilities of deep learning approaches if it outperforms the standard WPT denoising on the training class. As well, it will show how the L-WPT relates to the universality of signal processing if it follows better generalisation than deep NNs. Robustness analysis of our method is extended by considering different noise levels in sub-section V-E, noise types in sub-section V-F and some artifacts like offset and amplitude change in sub-section V-G. Finally we provide the impact of the main parameter of the L-WPT, the number of levels L , in the sub-section V-H.

A. Comparison to other approaches

We compare our method with a signal processing approach and several deep NNs. This will allow us to position our method with respect to the learning capabilities of deep models and the robustness of signal processing approaches.

We compare our framework to the hard thresholding wavelet shrinkage presented Section III-C. We call this method "Baseline-HT".

We consider the deep NNs presented in Section II: a standard CNN, a convolutional AE based on [18] and a U-Net model based on [49]. We provide in Appendix A-A a methodology to select the best AE architectures based on a set of pre-selected ones. In this case, the number of trainable parameters is extensive ($n_p = 554954$) compared to our L-WPT with 5 layers ($n_p = 1054$). To ensure that the results obtained are not mainly due to the difference in the number of parameters, causing the AE to overfit compared to the L-WPT, we also consider a similar AE architecture with the same number of parameters as the

L-WPT. We refer to those two architectures as "AE-large" and "AE-small".

We derive the architectures of the U-Net and CNN models from the two obtained AE architectures. We refer to them as "U-Net-large", "U-Net-small", "CNN-large" and "CNN-small".

The Table I provides an overview of the key parameters of the six different architectures. Unless stated otherwise, the activation function used at the output of each layer is the leaky ReLU with a leak of 0.1. The use of dropout and PRELU proposed in [19] was tested but abandoned because it decreased the performance.

The deep NNs are trained using exactly the same objective function optimisation parameters as the L-WPT (see Section IV-E).

B. Model functions and noise

We use the following benchmark case functions [9], which are named *Block*, *Bumps*, *HeaviSine* and *Doppler*. We propose to randomly generate signal classes s inspired by those four function cases. The number of samples in each signal s is set to $T = 2^{13}$. The definition of the four function classes is as follows:

- The *Block* class:

$$s(t) = \sum_{i=1}^{N_b} B(t, \tilde{\tau}_i, \tilde{w}_i, \tilde{\alpha}_i) \quad (15)$$

$$\text{with } B(t, \tau, w, \alpha) = \begin{cases} \alpha & \text{if } t \in [\tau - \frac{w}{2}, \tau + \frac{w}{2}], \\ 0 & \text{else} \end{cases} \quad (16)$$

The random parameters $\tilde{\tau}_i$ and \tilde{w}_i are respectively the center and the width of $N_b = 10$ block cutting the time axis of the signal s . Those blocks are generated by selecting randomly $N_b - 1$ samples t_2, t_3, \dots, t_{N_b} from 1 to T , listing them by increasing value and by fixing $t_1 = 0$ and $t_{N_b+1} = T$. Then $\tilde{\tau}_i = t_i + \tilde{w}_i/2$ and $\tilde{w}_i = t_{i+1} - t_i$. The amplitude $\tilde{\alpha}_i$ is a random variable generated from a normal distribution.

- The *Bumps* class:

$$s(t) = \sum_{i=1}^{N_b} B(t, \tilde{\tau}_i, \tilde{w}_i, \tilde{\alpha}_i) \quad (17)$$

$$\text{with } B(t, \tau, w, \alpha) = \frac{|\alpha|}{(1 + \frac{5}{w}|t - \tau|)^4} \quad (18)$$

The random variables and parameters are the same as in the *Block* class.

- The *HeaviSine* class:

$$s(t) = \sum_{i=1}^{N_b} B(t, \tilde{\tau}_i, \tilde{w}_i, \tilde{\alpha}_i, \tilde{f}_i, \tilde{\phi}_i) \quad (19)$$

$$\text{with } B = \begin{cases} |\alpha| \sin(\frac{ft}{200} + \phi) & \text{if } t \in [\tau - \frac{w}{2}, \tau + \frac{w}{2}], \\ 0 & \text{else} \end{cases} \quad (20)$$

For this case, we fix $N_b = 4$, the frequency variables \tilde{f}_i and the phase variable $\tilde{\phi}_i$ are both different realisations of a normal distribution.

- The *Doppler* class:

$$s(t) = \text{pad}_{\tilde{t}_p} \left[[t(t-1)]^{\frac{1}{2}} \sin \left(16\pi \frac{1+0.2}{20t+0.2} \right) \right] \quad (21)$$

where pad is a zero-padding function adding \tilde{t}_p 0 at the beginning of the signal, then inverting the function half of the realisations and cropping it, so it contains exactly T samples. The padding variable \tilde{t}_p is generated by selecting a random number from 0 to $T/2$, and the power variable \tilde{z} is generated by selecting a random number from 0 to 10

In order to keep the signals values in the same range, we normalize each realisation between 0 and 1 by performing the following transformation:

$$s(t) \leftarrow \frac{s(t) - s_{\min}}{s_{\max} - s_{\min}} \quad (22)$$

with s_{\min} and s_{\max} respectively the minimum and the maximum value of the current realisation s .

The pure signal \bar{s} is then corrupted by adding a white Gaussian noise, with \tilde{s} the corrupted signal. The corruption is performed as follows:

$$\tilde{s}(t) = 3s(t) + \sigma b(t) \quad (23)$$

where $b(t)$ is a realisation of a normal distribution, and σ is the noise level. The factor three is chosen to have an easier interpretation of the noise level, i.e., if $\sigma = 1$ almost all realizations will be in the same amplitude range as the pure signal ($\approx 99.7\%$ chances to be below 3).

- In Figure 4, we display different realisations of pure signals and their corrupted counterparts with $\sigma = 0.2$.

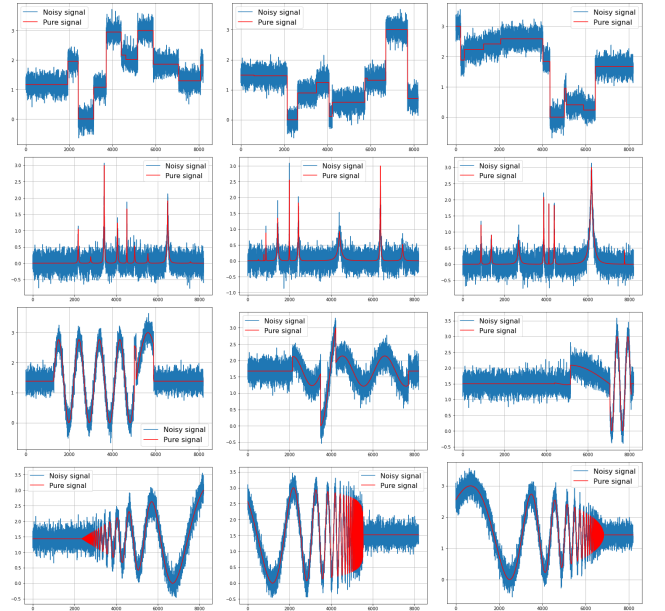


Fig. 4: Different realisations of the four function classes and their corrupted versions.

C. L-WPT training

To distinguish the differences between the L-WPT and the Baseline-HT method, we provide in Figure 5 the gain

CNN-large $n_p = 279649$				CNN-small $n_p = 736$			
Layers	Filters	Kernels	Comments	Layers	Filters	Kernels	Comments
Conv	32	20	No stride	Conv	8	10	No stride
Conv	64	15	No stride	Conv	16	5	No stride
Conv	128	10	No stride	Conv	8	8	No stride
Conv	256	5	No stride				
Conv	32	8	No stride				

AE-large $n_p = 554954$				AE-small $n_p = 1473$			
Layers	Filters	Kernels	Comments	Layers	Filters	Kernels	Comments
Conv	32	20	-	Conv	8	10	-
Conv	64	15	-	Conv	16	5	-
Conv	128	10	-	T-Conv	8	5	-
Conv	256	5	-	T-Conv	1	10	Lin act
T-Conv	128	5	-				
T-Conv	64	10	-				
T-Conv	32	15	-				
T-Conv	1	20	Lin act				

U-Net-large $n_p = 554954$				U-Net-small $n_p = 1473$			
Layers	Filters	Kernels	Comments	Layers	Filters	Kernels	Comments
Conv	32	20	SC	Conv	8	10	SC
Conv	64	15	SC	Conv	16	5	-
Conv	128	10	SC	T-Conv	8	5	-
Conv	256	5	-	T-Conv	1	10	Lin act
T-Conv	128	5	-				
T-Conv	64	10	-				
T-Conv	32	15	-				
T-Conv	1	20	Lin act				

TABLE I: The configuration of the six implemented neural network architectures. We used the following abbreviations: convolutional layer (Conv), transposed convolutional layer (T-Conv), linear activation function (Lin act), stride value is set to 1 (No stride), skip connection of the output to the related T-Conv layer (SC).

score presented in Section III-C when the L-WPT was trained on each class separately. The training was done on 16000 realisations \tilde{s} from one class with noise level $\sigma = 0.2$. We set the number of layers to $L = 5$. Contrary to the Baseline-HT case in Figure 2, the elimination of spurious information is not only a function of the amplitude, but also of its frequency content. The low frequencies are preserved, which seems to correspond to the fact that the four classes have a majority of low frequency content. Since the filters have no longer a high-low pass interpretation, the input cosinus can be modified in terms of frequency content. Unfortunately, this representation does not allow to show these modifications. However, it remains relevant to demonstrate that the behavior of L-WPT has been modified according to the training data.

D. Robust denoising

We compare the denoising properties of the L-WPT and the methods presented in this Section V-A. Thus, $N_{\text{test}} = 500$ test signals are generated for each class. We refer to the class used for the training as \mathbf{C}_T . We propose to evaluate the performance with respect to three scores: 1) the specialisation score denoted as S_p which shows how efficient a method is to denoise signals from \mathbf{C}_T ; 2) S_r the robustness score to demonstrate how the denoising performances are generalisable to the other classes; and 3) the mean score over all test signals, noted $\bar{S} = (S_p + 3S_r)/4$ that captures a trade-off between good specialisation and robustness. With \hat{s} the estimation of the

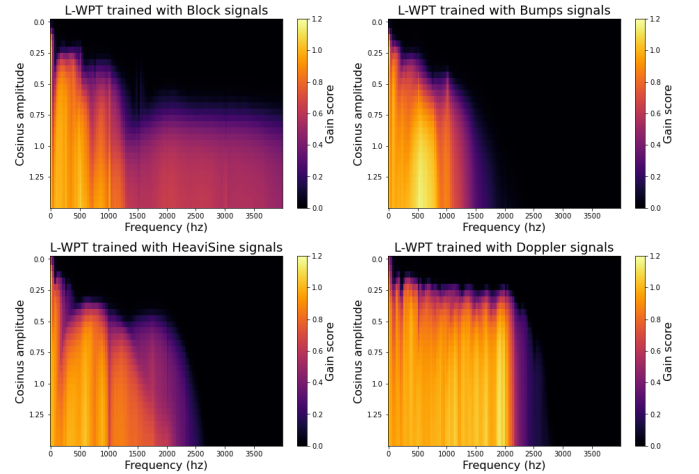


Fig. 5: Gain score from pure cosines signal with increasing frequency and amplitude for the L-WPT trained with a different function class.

pure signal s , the computation of S_p and S_r is derived as follows:

$$S_p = \frac{10^5}{TN_{\text{test}}} \sum_{i/s_i \in \mathbf{C}_T} \|\hat{s}_i - s_i\|_F^2 \quad (24)$$

$$S_r = \frac{10^5}{3TN_{\text{test}}} \sum_{i/s_i \notin \mathbf{C}_T} \|\hat{s}_i - s_i\|_F^2 \quad (25)$$

In Table II, the S_p , S_r and \bar{S} scores for the cases when each model is trained using the four classes separately are

displayed. The AE-large model has the best specialization performance. However, the method does not generalise well to the other classes. This is reflected in its S_r score for the Bumps and Doppler classes. Overall, the L-WPT has the best robustness score, even better than the Baseline-HT method that is particularly adapted for Gaussian denoising. We can state that, for this experiment, the L-WPT keeps the robustness of a general, non trainable denoising procedure like the Baseline-HT, but also learns a relevant denoising for the signals of the learned class.

In Figure 6, the denoising obtained for the AE-large and L-WPT for one realisation of each class when the methods are trained using this class is displayed. In this case, AE-large performs the best. This can be shown by considering the absolute error between the estimated and the pure signal through time.

The Figure 7 can be seen as a table of figures, where the columns provide a zoom of the four considered signals from Figure 6, and the rows provide the output of the L-WPT and AE big when they are trained with each of the four classes. We can see that the AE-large performs poorly when it is trained using another class. This is particularly easy to observe for the Doppler case.

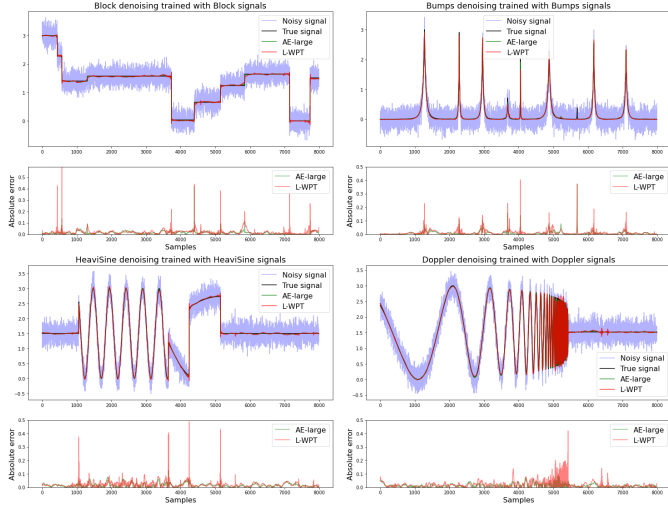


Fig. 6: (Top) Denoising with L-WPT and AE-large when they are trained using the corresponding class function. (Bottom) Absolute error between the denoised signal and the ground truth.

E. Impact of the noise level

In practical applications, noise levels can change over time. This can for example occur under new operating conditions or if the training was done combining signals and background with specified SNR [19]. In our setup, the training noise level is fixed to $\sigma = 0.2$. We then quantify the performance of each method for different values of the noise level.

The S_p , S_r and \bar{S} scores are computed again when the noise level takes the values $\{0.1, 0.4, 0.6, 0.8, 1\}$. Since the thresholds learned for the L-WPT are fixed to perform

well for $\sigma = 0.2$, there is no particular reason that it will continue to do a relevant denoising for other noise levels. To adjust the weights, we perform the L-WPT- (δ) transformation introduced in Section IV-A with $\delta = \frac{\sigma}{\sigma_{\text{train}}} = 5\sigma$. Here, we assume we have a good estimation of the noise level for the new operating condition. In order to highlight the denoising performance of our L-WPT- (δ) method, we compute again the best threshold of the Baseline-HT method for each noise level.

Figure 8 shows the specialisation and the robustness scores for each method, for the different noise levels and for each training class. We display the decimal logarithmic value of the scores in order to ease the reading of the graphs. The L-WPT performs poorly. However, the modified version with the weight adjustment outperforms all other methods. In the case of $\sigma = 1$, the L-WPT- (5σ) method can provide an up to 10-times better denoising capability compared to the deep NN models.

The L-WPT- (δ) also outperforms the Baseline-HT method where the threshold was optimised to the new level of noise. It demonstrates that the filters learned by L-WPT are robust to higher levels of noise and that only the biases need to be adjusted.

The Figure 6 demonstrates the denoising performance of L-WPT- (5σ) compared to the AE-large method for the test signal with $\sigma = 1$ (both methods are trained using the class on which they are also tested: specialization regime).

F. Impact of noise type

If the operating conditions are changing, not only the noise level may be impacted but also the type of the noise. We evaluate this by computing the S_p , S_r and \bar{S} scores on test signals with noise of different levels and different types. We consider a uniform noise between $[-\frac{\sqrt{12}}{2}, \frac{\sqrt{12}}{2}]$ (the $\sqrt{12}$ factor is used to adjust the variance of the uniform noise to the normal distribution). We also consider the Laplace distribution that has a heavier tail compared to the Gaussian distribution. This means that more outliers will be generated. The used Laplace distribution has a mean of 0 and the scale parameter $1/\sqrt{2}$ (to adjust the variance to the normal distribution).

Table III provides an overview of the average of the S_p , S_r and \bar{S} scores over the four classes for different combinations of noise levels and types. Similarly to the Gaussian case, the L-WPT- (5σ) is robust to different background noise levels and types and it outperforms all other methods.

G. Robustness to test functions offset and amplitude modifications

Finally, we consider small transformations of the pure signal. They differ slightly from the ones of the training dataset. In a first case, we consider input signal with an offset. We refer to the transformation applied to all test signals s as $M(s)$. We consider the following cases: $M(s) = s + 1.5$ and $M(s) = s - 1.5$. This will show how the methods react to new signal values that were never seen in

Method	Block			Bump			HeaviSine			Doppler			Mean results		
	S_p	S_r	\bar{S}	S_p	S_r	\bar{S}	S_p	S_r	\bar{S}	S_p	S_r	\bar{S}	S_p	S_r	\bar{S}
Baseline-HT	354	246	273	194	300	273	225	291	274	317	260	275	273	274	274
AE-large	24	577	439	20	1859	1399	33	563	431	36	1575	1190	28	1143	865
AE-small	127	332	281	56	706	544	129	383	319	233	226	228	136	412	343
CNN-large	75	355	285	39	965	734	75	355	285	94	305	252	71	495	389
CNN-small	189	329	294	79	624	488	195	342	305	270	259	262	183	389	337
Unet-large	27	423	324	21	1508	1136	35	309	240	36	810	617	30	763	579
Unet-small	136	339	288	61	646	499	133	352	297	201	230	223	133	392	327
L-WPT	83	315	257	43	358	279	56	195	161	98	143	132	70	253	207

TABLE II: specialisation score (S_p), robustness score (S_r) and (\bar{S}) mean score over the 4 function types when methods are trained using only the classes of the corresponding column.

Method	uniform $\sigma = 0.2$			Uniform $\sigma = 0.4$			Uniform $\sigma = 1$			Laplace $\sigma = 0.2$			Laplace $\sigma = 0.4$			Laplace $\sigma = 1$		
	S_p	S_r	\bar{S}	S_p	S_r	\bar{S}	S_p	S_r	\bar{S}	S_p	S_r	\bar{S}	S_p	S_r	\bar{S}	S_p	S_r	\bar{S}
Baseline-HT	268	270	269	859	866	864	4955	5049	5025	282	284	283	906	916	913	5336	5449	5420
AE-large	28	1143	864	319	1395	1126	7360	9996	9337	36	1141	865	623	1472	1259	9046	1.0e4	1.0e4
AE-small	135	410	341	1019	1372	1284	2.2e4	2.8e4	2.7e4	144	418	350	1328	1638	1560	2.4e4	3.1e4	2.9e4
CNN-large	70	496	389	595	1015	910	1.2e4	1.0e4	1.1e4	80	495	391	1039	1168	1136	1.6e4	1.2e4	1.3e4
CNN-small	181	387	336	1202	1458	1394	2.2e4	2.0e4	2.0e4	191	393	343	1493	1590	1566	2.2e4	2.0e4	2.0e4
Unet-large	29	763	579	435	1120	949	1.0e4	9882	1.0e4	39	763	582	934	1281	1194	1.2e4	1.0e4	1.1e4
Unet-small	131	390	325	1183	1506	1425	2.1e4	2.1e4	2.1e4	142	398	334	1529	1723	1675	2.2e4	2.2e4	2.2e4
L-WPT-(δ)	69	250	205	256	686	578	1808	2894	2622	80	266	220	330	773	662	2509	3684	3390

TABLE III: Mean results over the four classes of the specialisation score (S_p), robustness score (S_r) and mean score (\bar{S}) in function of different kind of noise and noise level when each model were trained with a gaussian noise of level $\sigma = 0.2$.

Method	$M(f) = f + 1.5$			$M(f) = f - 1.5$			$M(f) = 2f$			$M(f) = 0.5f$		
	S_p	S_r	\bar{S}	S_p	S_r	\bar{S}	S_p	S_r	\bar{S}	S_p	S_r	\bar{S}
Baseline-HT	271	273	273	306	312	310	362	364	364	219	221	221
AE-large	303	994	821	96751	121739	115492	474	5435	4195	80	333	270
AE-small	225	465	405	57320	29480	36440	277	1210	977	133	214	194
CNN-large	1950	1478	1596	67649	47435	52488	6827	5012	5466	104	232	200
CNN-small	317	461	425	68125	58080	60591	524	870	783	205	252	240
Unet-large	3527	2546	2792	60596	47823	51016	14974	10853	11884	71	288	234
Unet-small	266	447	401	83004	122679	112760	234	986	798	144	220	201
L-WPT	119	320	270	140	250	223	121	468	381	62	165	139

TABLE IV: Mean results over the four classes of the specialisation score (S_p), robustness score (S_r) and mean score (\bar{S}) in function of different kind of function deformation when each normal where trained with the identity modification function.

the training dataset. We also consider signals with different scales, i.e. $M(s) = 2s$ and $M(s) = 0.5s$.

Similarly as before, the baseline-HT has its threshold optimised to provide the best denoising for each modification.

Table III shows the average the S_p , S_r and \bar{S} scores over the four classes for the different modification functions. We can see how the deep NNs generalize very poorly to the transformation with negative offset. Indeed in the training dataset, the negative values were only associated with noise. Overall, the L-WPT outperforms all deep-learning models with respect to the robustness and also the specialisation score. Only when the input signal contains large value (cases $M(s) = s + 1.5$ and $M(s) = 2s$), the baseline-HT appears to be more robust. However, the L-WPT stays consistent.

H. Impact of the number of layers

We evaluate the impact of different number of layers on the performance of L-WPT. Figure V displays the S_p , S_r and \bar{S} scores obtained using trained L-WPT with different number of layers L . Results for Doppler, HeaviSine and Blocks classes stay consistent independently of the number of layers. However, for the Bumps case, we have a considerable decrease of robustness when the number of

layers is higher than six. It shows than L-WPT can also overfit if we use too specific signals for the training. To tackle this issue, we recommend to use a number of layers between 4 and 6 to avoid having too many parameters, or to add in the training dataset dummy signal like pure cosines to limit the loss of the WPT properties.

VI. APPLICATION ON AUDIO BACKGROUND DENOISING

We evaluate the proposed L-WPT on denoising real signals. For this case study, we also compare to the same methods presented in subsection V-A. The alternative methods are the Baseline-HT, AE-large, AE-small, CNN-large, CNN-small, UNet-large and UNet-small. For the deep NNs models, we use the same architecture as reported in Table I. The justification of this choice is provided in Appendix A-B.

After presenting the dataset in subsection VI-A, an analysis of the trained L-WPT for the airport background removal is provided in subsection VI-B. The denoising performance of each method is reported in subsection VI-C with respect to the robustness and specification score. For this case, the SNR is known and an application on real conditions with unknown SNR is provided in subsection VI-D. We provide in this subsection a method to estimate the δ value of the δ transform.

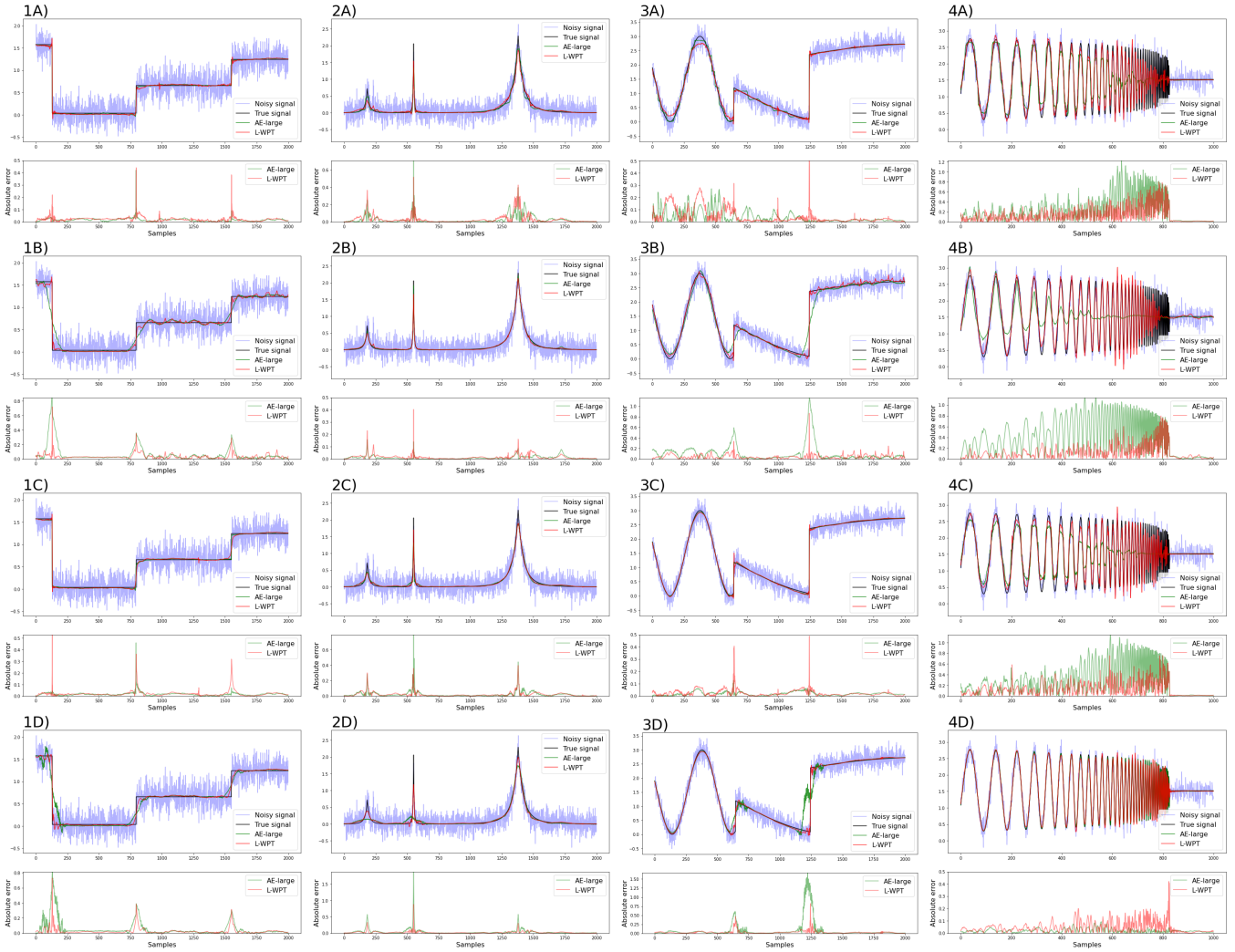


Fig. 7: Table of figures showing denoising examples for the AE-large and L-WPT methods. The numbers one to four and the letter A to D represent respectively the Block, Bumps, HeaviSine and Doppler classes, the number is the represented class where the letter is the class used to train the model.

WPT-L layers	Block			Bump			HeaviSine			Doppler			Mean results		
	S_p	S_r	\bar{S}	S_p	S_r	\bar{S}	S_p	S_r	\bar{S}	S_p	S_r	\bar{S}	S_p	S_r	\bar{S}
4	91	281	233	49	397	310	64	178	150	127	130	129	83	246	206
5	83	315	257	43	358	279	56	195	161	98	143	132	70	253	207
6	68	188	158	41	846	645	47	179	146	88	145	131	61	339	270
7	67	220	182	40	2770	2088	44	166	136	78	166	144	57	830	637
8	70	214	178	40	1689	1276	45	168	137	81	210	178	59	570	442

TABLE V: specialisation score (S_p), robustness score (S_r) and (\bar{S}) mean score over the 4 function types in function of the number of layers in the L-WPT.

A. Dataset

We consider the dataset from the task 1 and 2 of the DCASE 2018 challenge [50], [51]. The first dataset provides acoustic scenes that are used as noisy backgrounds. We only consider the scenes of the airports of Barcelona, Helsinki, London, Paris and Stockholm. The second task provides a variety of 41 different foreground sound events like "Cello", "Bus" or "Bark". We randomly eliminated the "Trumpet" classes in order to keep only 40 different classes and ease the division of the dataset into folds. We consider only signals where the classe label have been checked manually.

The background training signals are based on 102 10-seconds recordings of the Barcelona airport scene only, the test background uses 26 different recordings of the Barcelona airport or the recordings of the other airport scenes. Moreover, the foreground training signals are based on 3610 recordings, different from the 1600 recordings used for the test classes.

For the audio signal generation of the foreground and background signals, we apply a similar strategy as in [19]. The recordings are downsampled to 8 kHz, cropped randomly in order to have signals with $T = 2^{13}$ samples,

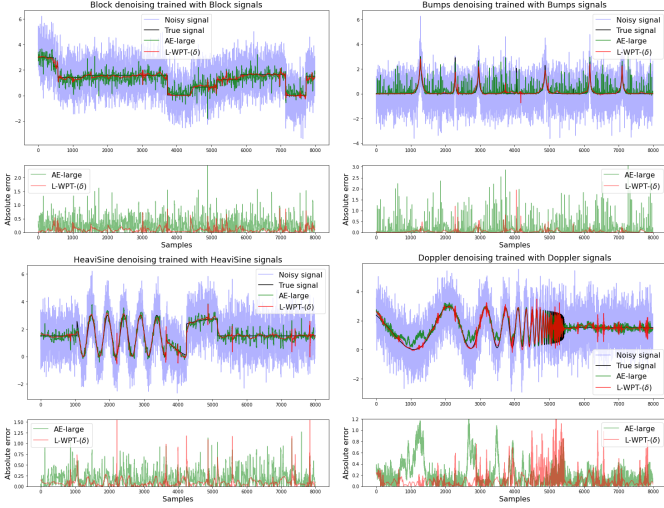


Fig. 8: (Top) Denoising with L-WPT (weight mult) and AE-large when they are trained using the corresponding class function with a noise level of $\sigma = 0.2$ and tested on a noise level of $\sigma = 1$. (Bottom) Absolute error between the denoised signal and the ground truth

and normalized. For the foreground sound, we apply padding and make sure that the random cropping does not select a null signal. We mix the foreground and background sound by adding them, the signal to noise ratio in this case is 0 dB. For the training, new signals are continuously generated from the training recordings. 1600 test signals are generated from the test recordings

The methods are not trained on all the classes directly, the data is cut into 8 folds of 5 classes each. This aims to mimic real world applications: A limited amount of classes is collected and used for training the model. The trained model is then applied in a more general environment where we aim to eliminate the background also for classes of signals different from the training data.

B. Details of the L-WPT training

We consider the L-WPT with eight layers. It corresponds to the number of layers minimising the entropy for the WPT when applied to the pure signals of the first fold, the entropy minimisation is a standard method used to select the best number of layers [52].

Figure 10 visualizes the gain scores using cosines of different amplitudes and frequency as in Section III-C for the first three folds. We can see that even if each L-WPT was trained using the signals from different classes, the gain scores images appear to be relatively similar. The left Figure 10 shows the average spectrum (in absolute values and in Decibels (DB)) of the training background noise. We can see that it contains mostly low frequency contents from 0 to 800 Hz. It is interesting to remark that the gain score for cosines with a low frequency content from 0 to 800 Hz stays null for higher amplitudes than cosines with a higher frequency. It shows how the L-WPT learned to suppress the background contents. For the highest frequencies (>3500),

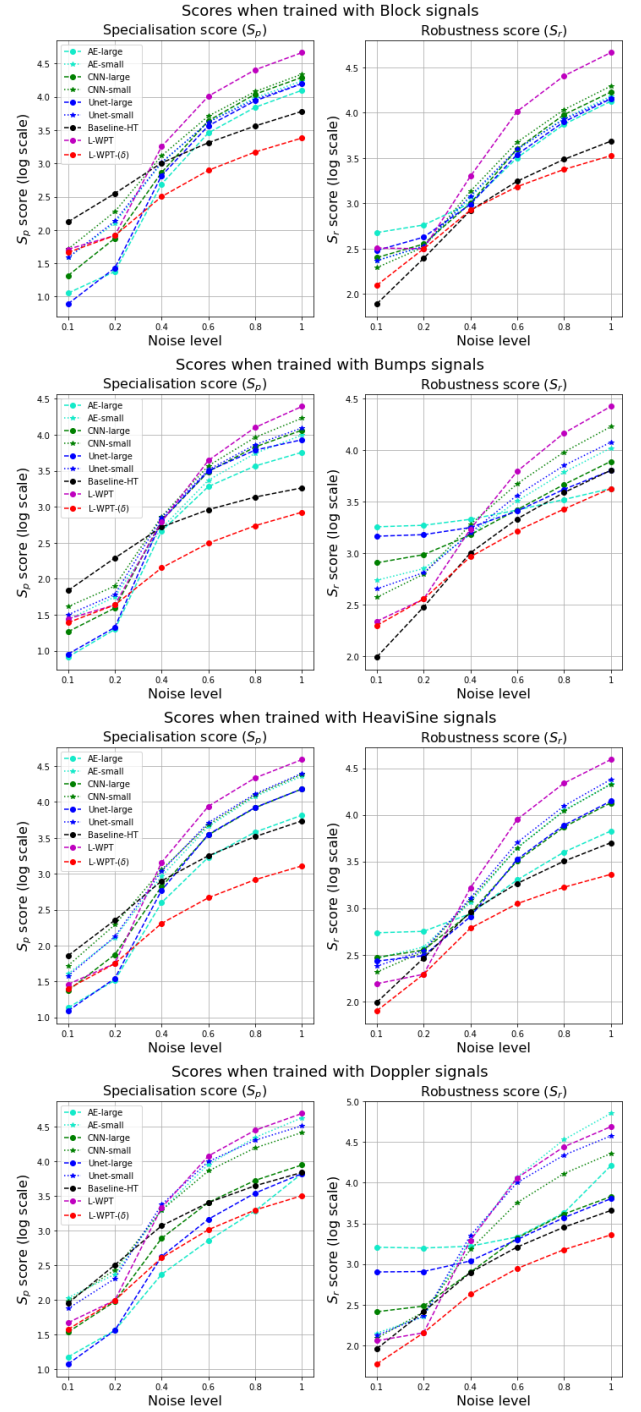


Fig. 9: Logarithm of the S_p and S_r scores through different noise level for each method when trained using a noise level of $\sigma = 0.2$.

the background content is almost null and it turns out that the gain scores are more heterogeneous from one fold to another. It implies the L-WPT were more able to specialise to the training fold for non-corrupted frequency bands.

C. Robust background removal

The S_p , S_r and \bar{S} scores introduced in Section V-C are also applied in this case study, where the training classes

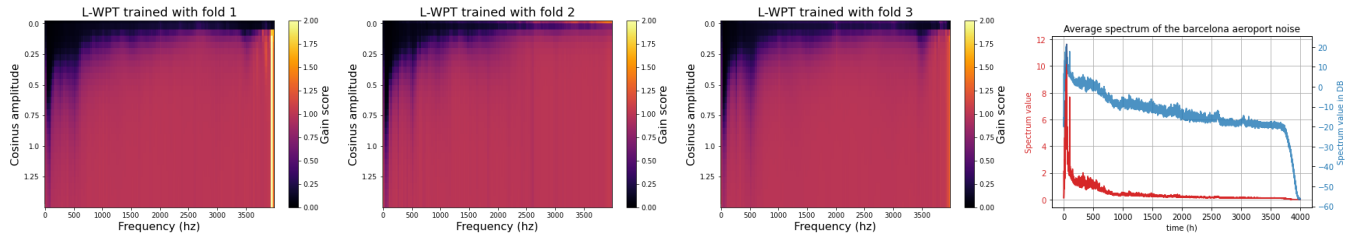


Fig. 10: (Three left) Gain score from pure cosines signal with increasing frequency and amplitude for the WPT and the L-WPT tfor the three first folds. (right) Mean spectrogram (modulus and decibels) of the barcelona airport noise signals

C_{train} are the 5 classes of the current fold. We also consider the mean square error between the estimated and pure signals obtained for each class separately.

Figure 11 shows the normalised mean square error obtained for each class when the L-WPT and the AE-large were trained with the fold 1 and 2. The classes belonging to C_{train} are displayed in red, the difference between the scores obtained with L-WPT and AE-large is highlighted in green when L-WPT performs best and in purple when AE-large performs best. For this experiment, the L-WPT almost always outperforms the AE-large. The gap between the L-WPT and the AE-large MSE is reduced for C_{train} . For example in the fold 2, the MSE is reduced by 2.6 on average for all classes, whereas it is reduced only by 0.6 if we only consider the training class. It shows how our method is able to generalize well to structured signal from classes different from the training dataset.

Figure 13 shows an example of denoising with L-WPT and AE-large when they were trained with the fold 1. The two first cases, "Glockenspiel" and "Harmonica" signals, are cases where the L-WPT performs particularly well compared to the AE-large. The last case "Drawer open and close" is a case where both methods perform similarly. In this last case, the AE-large performs better in eliminating noise alone, however, the L-WPT is slightly more accurate in reconstructing the sound of interest (as indicated by the absolute error).

In Table VI, the mean S_p , S_r and \bar{S} scores over the 8 folds and for each method are provided. The score is obtained for the Bacerlona airport scene background sounds and the other airport sounds. We recall that the training data use only background sounds from the Barcelona airport. Because the background noise contains specific frequency contents, the baseline-HT method is no longer adapted since it denoises each frequency bands in the same way. It, therefore, gives poor results. Overall, the L-WPT outperforms all other methods. For the airport case, the gap between the specialisation score and the robustness score is 0.5 which is low. However, the AE-large has a gap between the specialisation score and the robustness score of 2.4 which is comparable large. This demonstrates again that L-WPT has the learning capabilities of deep NNs while keeping the universal properties of signal processing. Considering the background of other airports, the trend is similar, with L-WPT outperforming the other methods in terms of specialization and robustness scores. It also

shows that there are not many differences between the background sounds of different airports.

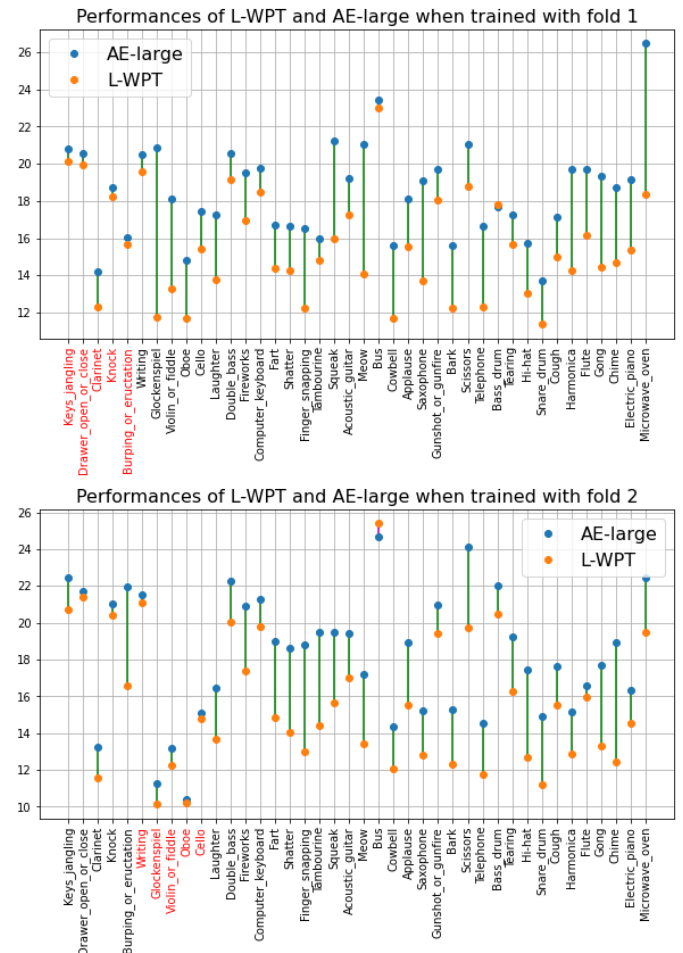


Fig. 11: Performances of the AE-large and L-WPT for each classes when they are trained using three different folds. The classes belonging to C_{train} are in red, the difference between the score obtained via L-WPT and AE-large is highlighted in green when L-WPT works best, in purple when AE-large works best.

D. Real conditions application with unknown SNR

Each method was trained based on corrupted signals with a fixed SNR. However, the denoising performances can decrease if applied in real applications to sounds with

Method	Barcelona			Helsinki			London			Paris			Stockholm		
	S_p	S_r	\bar{S}	S_p	S_r	\bar{S}	S_p	S_r	\bar{S}	S_p	S_r	\bar{S}	S_p	S_r	\bar{S}
Baseline-HT	28.2	28.4	28.4	28.3	28.4	28.4	28.1	28.2	28.2	28.4	28.2	28.2	28.1	28.1	28.1
AE-large	14.9	17.3	17.0	14.8	17.3	17.0	15.8	18.0	17.7	15.2	17.6	17.3	15.8	18.1	17.8
AE-small	21.3	22.6	22.5	20.7	22.1	21.9	21.6	22.9	22.7	21.2	22.5	22.3	21.4	22.7	22.5
CNN-large	16.7	18.3	18.1	16.4	18.0	17.8	17.2	18.7	18.5	16.8	18.4	18.2	17.0	18.5	18.4
CNN-small	18.3	18.9	18.8	17.6	18.3	18.2	18.4	19.0	18.9	18.0	18.7	18.6	18.2	18.9	18.8
Unet-large	16.2	19.0	18.7	16.1	19.0	18.6	17.2	19.8	19.5	16.6	19.4	19.0	17.1	19.8	19.4
Unet-small	17.6	18.3	18.2	16.9	17.6	17.5	17.9	18.5	18.4	17.4	18.1	18.0	17.6	18.3	18.2
L-WPT	14.3	14.8	14.8	13.7	14.3	14.2	15.1	15.6	15.6	14.3	14.8	14.8	15.1	15.6	15.6

TABLE VI: specialisation score (S_p), robustness score (S_r) and mean score (\bar{S}) over the 8 folds when each method are trained with the Barcelona noise only.

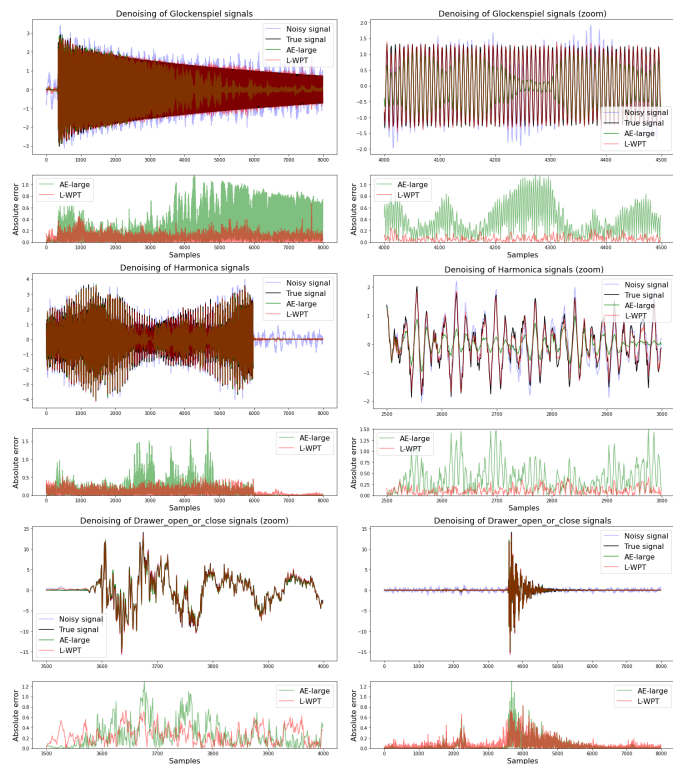


Fig. 12: (Top) Denoising with L-WPT (weight mult) and AE-large when they are trained using the fold one. (Bottom) Absolute error between the denoised signal and the ground truth

different SNR. Indeed, depending on the location of the sensor in the airport or the recording time, the SNR can differ significantly. Thus, we now consider different SNR for the test signal. For this, we use the non-normalised airport background noises. Since their raw value ranges are too low compared to the signals of interest, we multiplied them by 200. These values are chosen so that the majority of signals has a higher SNR than for the training case. This corresponds to the situation where the denoising can be impaired.

We impose that the first 2000 samples of the test signals contain only the background noise. Thereby, it is possible to evaluate the δ value for the L-WPT- δ transformation. The δ value is defined as the fraction between the norm of the 2000 first samples over the average norm when we select randomly 2000 samples from the background of the

Method	Barcelona		
	S_p	S_r	\bar{S}
AE-large	19.3	21.5	21.2
AE-small	26.2	27.4	27.3
CNN-large	21.6	23.1	22.9
CNN-small	23.3	23.9	23.8
Unet-large	19.8	22.6	22.2
Unet-small	22.8	23.4	23.3
L-WPT-(δ)	18.5	18.9	18.9

TABLE VII: specialisation score (S_p), robustness score (S_r) and mean score (\bar{S}) over the 8 folds when each method are trained with the Barcelona noise at 0db, the test dataset has varying noise SNR.

training dataset. The idea is to see if the background energy of the current recording is higher or lower than from the training dataset.

Figure 13 shows the histograms of the obtained δ values over the 1600 recordings of the test dataset. On average, the value of δ is larger than one. This means that the SNR for the test dataset is negative. Table VII shows the S_p , S_r and \bar{S} results for each of the applied deep NN architectures. The extended L-WPT- δ outperforms other methods with respect to each of the scores. It shows again how the L-WPT learn kernels that are robust to different noise level. Thus, the L-WPT can be easily adapted to different operating conditions by modifying the biases only.

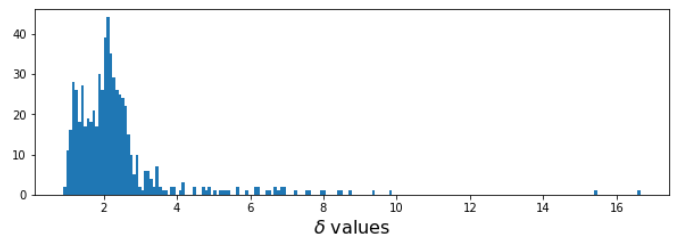


Fig. 13: Frequency of δ values modifying the bias of the L-WPT-(δ) method over the test dataset

VII. CONCLUSION

In this paper, we propose to combine two of the main signal denoising tools: Wavelet shrinkage using wavelet packet transform and supervised denoising by a convolutional autoencoder. Our proposed learnable WPT is interpretable, relying on the signal processing properties of WPT while being able to learn the specifics of the training dataset.

Moreover, it is able to generalize to different classes of the training dataset. It has an intuitive parameter initialization that allows it to initialize like a wavelet packet transform. Moreover, we propose a powerful post-learning modification of the weights, called the δ -modification. This modification is only possible because the meaning of each parameter in this architecture is known. Thus, it is possible to adapt denoising to different noise levels resulting from different operating conditions.

The L-WPT is compared to deep supervised models and the WPT denoising in two experiments. It was first applied on case functions often used in the denoising literature. The L-WPT was able to learn specific denoising for the signals in the training class. Furthermore, we demonstrate that it retains the robustness of a universal signal processing procedure by testing it on noisy signals outside the training class. We also show that our method was also robust to different types and levels of noise thanks to the δ -modification. Finally, the L-WPT method was applied to a background suppression task and performed better than the other methods. We provide a recommendation for using the δ -modification in a real-world application that has been shown to be effective for background denoising in a variable SNR.

This work opens several doors for future directions. First, further research on the δ -modification or related modifications should be conducted. For example, learning the L-WPT on different noise levels would show if the kernels remain similar. This would tell us how optimal the δ -modification is. Another future direction would be to use the time-frequency representation of L-WPT as a feature for a supervised task instead of the WPT features. On the application side, it would be interesting to apply our approach in the context of speech enhancement with a fixed background. Finally, the generalization of our approach to multi-dimensional signals would lead to its application to image denoising.

APPENDIX A

A. Choice of the NN architectures: case function model

We aim to adapt the AE architecture from [18] to our case, the main differences being the number of input samples. The Table VIII shows at the columns "Function", the obtained specialisation score (S_p), robustness score (S_r) and (\bar{S}) mean score for different set of architectural choices. The number of filters for each layers is given in the first column, the kernel size has 5 coefficients in the last layer and increases by 5 for each outer layer. We can remark the robustness score decreases as the number of parameters increase. The architecture [16-32-64-128-256] has the best specialisation score ($S_p=22$) compared to [32-64-128-256] with $S_p=24$. However, we select the later architecture because it is way more robust ($S_r=577$ vs $S_r=919$) compared to the small gain in specialisation.

Architecture	Function			Background		
	S_p	S_r	\bar{S}	S_p	S_r	\bar{S}
[16-32-64]	46	427	332	18.5	17.8	17.9
[32-64-128]	45	430	334	17.7	17	17.2
[64-128-256]	45	434	337	18.2	17.9	18
[16-32-64-128]	25	590	448	17.1	17.7	17.7
[32-64-128-256]	24	577	439	16.9	17.1	17
[64-128-256-512]	54	663	510	19	20	19.9
[16-32-64-128-256]	22	919	694	21.1	26	25.4
[32-64-128-256-512]	118	1058	823	21.6	25.5	25

TABLE VIII: Specialisation (S_p), robustness (S_r) and mean (\bar{S}) score for the Block function ("Function") and for the first fold of the background denoising case ("Background").

B. Choice of the NN architectures: airport background removal

The Table VIII column "Background", shows the experiment from Appendix A-A applied to the first fold of the Background denoising task. We choose the architecture [32 – 64 – 128 – 256] because it provides the best S_p score and close to the best S_r score.

We introduced AE-small as an AE architecture with similar number of parameters than L-WPT. However, the L-WPT with $L = 8$ contains more parameters ($n_p = 8670$) than when $L = 5$. For simplicity, we keep using then the small architectures from Table I. Indeed, we also tried three architectures with number of parameters around $n_p = 8670$: [16-32] with $n_p = 5488$, [8-16-32] with $n_p = 6632$ and [32-64] with $n_p = 21216$. The best performing is the [32-64] with $S_p = 19.3$ and $S_r = 19.5$ for the first fold. It outperforms the AE-small ($S_p = 21.9$, $S_r = 22$, 4) but does worse than AE-large anyway ($S_p = 16.9$, $S_r = 17.1$).

REFERENCES

- [1] H. Li and F. Liu, "Image denoising via sparse and redundant representations over learned dictionaries in wavelet domain," in *2009 Fifth International Conference on Image and Graphics*. IEEE, 2009, pp. 754–758.
- [2] Y. Li, C. Xu, L. Yi, and R. Fang, "A data-driven approach for denoising gnss position time series," *Journal of Geodesy*, vol. 92, no. 8, pp. 905–922, 2018.
- [3] S. K. Jha and R. Yadava, "Denoising by singular value decomposition and its application to electronic nose data processing," *IEEE Sensors Journal*, vol. 11, no. 1, pp. 35–44, 2010.
- [4] A. Rajwade, A. Rangarajan, and A. Banerjee, "Image denoising using the higher order singular value decomposition," *IEEE Transactions on Pattern Analysis and Machine Intelligence*, vol. 35, no. 4, pp. 849–862, 2012.
- [5] G. Frusque, M. Gabriel, and F. Olga, "Canonical polyadic decomposition and deep learning for machine fault detection," in *PHM Society European Conference*, vol. 6, no. 1, 2021, pp. 9–9.
- [6] J. Xie, J. G. Colonna, and J. Zhang, "Bioacoustic signal denoising: a review," *Artificial Intelligence Review*, vol. 54, no. 5, pp. 3575–3597, 2021.
- [7] B. Goyal, A. Dogra, S. Agrawal, B. S. Sohi, and A. Sharma, "Image denoising review: From classical to state-of-the-art approaches," *Information fusion*, vol. 55, pp. 220–244, 2020.
- [8] F. M. Bayer, A. J. Kozakevicius, and R. J. Cintra, "An iterative wavelet threshold for signal denoising," *Signal Processing*, vol. 162, pp. 10–20, 2019.
- [9] D. L. Donoho and J. M. Johnstone, "Ideal spatial adaptation by wavelet shrinkage," *biometrika*, vol. 81, no. 3, pp. 425–455, 1994.
- [10] S. Zhou, J. Tang, C. Pan, Y. Luo, and K. Yan, "Partial discharge signal denoising based on wavelet pair and block thresholding," *IEEE Access*, vol. 8, pp. 119 688–119 696, 2020.

- [11] A. Kumar, H. Tomar, V. K. Mehla, R. Komaragiri, and M. Kumar, "Stationary wavelet transform based ecg signal denoising method," *ISA transactions*, vol. 114, pp. 251–262, 2021.
- [12] Z. A. A. Alyasseri, A. T. Khader, M. A. Al-Betar, A. K. Abasi, and S. N. Makhadmeh, "Eeg signals denoising using optimal wavelet transform hybridized with efficient metaheuristic methods," *IEEE Access*, vol. 8, pp. 10 584–10 605, 2019.
- [13] S. G. Chang, B. Yu, and M. Vetterli, "Adaptive wavelet thresholding for image denoising and compression," *IEEE transactions on image processing*, vol. 9, no. 9, pp. 1532–1546, 2000.
- [14] K. Zhang, W. Zuo, Y. Chen, D. Meng, and L. Zhang, "Beyond a gaussian denoiser: Residual learning of deep cnn for image denoising," *IEEE transactions on image processing*, vol. 26, no. 7, pp. 3142–3155, 2017.
- [15] S. A. Nossier, J. Wall, M. Moniri, C. Glackin, and N. Cannings, "A comparative study of time and frequency domain approaches to deep learning based speech enhancement," in *2020 International Joint Conference on Neural Networks (IJCNN)*. IEEE, 2020, pp. 1–8.
- [16] C. T. Arsene, R. Hankins, and H. Yin, "Deep learning models for denoising ecg signals," in *2019 27th European Signal Processing Conference (EUSIPCO)*. IEEE, 2019, pp. 1–5.
- [17] T. Kounovsky and J. Malek, "Single channel speech enhancement using convolutional neural network," in *2017 IEEE International Workshop of Electronics, Control, Measurement, Signals and their Application to Mechatronics (ECMSM)*. IEEE, 2017, pp. 1–5.
- [18] X. Liu, Q. Zhou, J. Zhao, H. Shen, and X. Xiong, "Fault diagnosis of rotating machinery under noisy environment conditions based on a 1-d convolutional autoencoder and 1-d convolutional neural network," *Sensors*, vol. 19, no. 4, p. 972, 2019.
- [19] S. A. Nossier, J. Wall, M. Moniri, C. Glackin, and N. Cannings, "An experimental analysis of deep learning architectures for supervised speech enhancement," *Electronics*, vol. 10, no. 1, p. 17, 2020.
- [20] M. Ravanelli and Y. Bengio, "Speaker recognition from raw waveform with sincnet," in *2018 IEEE Spoken Language Technology Workshop (SLT)*. IEEE, 2018, pp. 1021–1028.
- [21] J. Xin, J. Li, X. Jiang, N. Wang, H. Huang, and X. Gao, "Wavelet-based dual recursive network for image super-resolution," *IEEE Transactions on Neural Networks and Learning Systems*, 2020.
- [22] F. Gaëtan and F. Olga, "Learnable wavelet packet transform for data-adapted spectrograms," in *ICASSP 2022 - 2022 IEEE International Conference on Acoustics, Speech and Signal Processing (ICASSP)*, 2022, pp. 3119–3123.
- [23] G. Michau and O. Fink, "Fully learnable deep wavelet transform for unsupervised monitoring of high-frequency time series," *arXiv preprint arXiv:2105.00899*, 2021.
- [24] R. Hidayat, A. Bejo, S. Sumaryono, and A. Winursito, "Denoising speech for mfcc feature extraction using wavelet transformation in speech recognition system," in *2018 10th International Conference on Information Technology and Electrical Engineering (ICITEE)*. IEEE, 2018, pp. 280–284.
- [25] Ç. P. Dautov and M. S. Özerdem, "Wavelet transform and signal denoising using wavelet method," in *2018 26th Signal Processing and Communications Applications Conference (SIU)*. IEEE, 2018, pp. 1–4.
- [26] M. A. Oktar, M. Nibouche, and Y. Baltaci, "Speech denoising using discrete wavelet packet decomposition technique," in *2016 24th Signal Processing and Communication Application Conference (SIU)*. IEEE, 2016, pp. 817–820.
- [27] G. Kumar, S. Kumar, and N. Kumar, "Comparative study of wavelet and wavelet packet transform for denoising telephonic speech signal," *International Journal of Computer Applications*, vol. 110, no. 15, 2015.
- [28] M. Schimmack and P. Mercorelli, "Noise detection for biosignals using orthogonal wavelet packet tree denoising algorithm," *International Journal of Electronics and Telecommunications*, vol. 62, no. 1, pp. 15–21, 2016.
- [29] —, "A wavelet packet tree denoising algorithm for images of atomic-force microscopy," *Asian Journal of Control*, vol. 20, no. 4, pp. 1367–1378, 2018.
- [30] C. Beale, C. Niezrecki, and M. Inalpolat, "An adaptive wavelet packet denoising algorithm for enhanced active acoustic damage detection from wind turbine blades," *Mechanical Systems and Signal Processing*, vol. 142, p. 106754, 2020.
- [31] G.-d. Yue, X.-s. Cui, Y.-y. Zou, X.-t. Bai, Y.-H. Wu, and H.-t. Shi, "A bayesian wavelet packet denoising criterion for mechanical signal with non-gaussian characteristic," *Measurement*, vol. 138, pp. 702–712, 2019.
- [32] S.-W. Fu, Y. Tsao, X. Lu, and H. Kawai, "Raw waveform-based speech enhancement by fully convolutional networks," in *2017 Asia-Pacific Signal and Information Processing Association Annual Summit and Conference (APSIPA ASC)*. IEEE, 2017, pp. 006–012.
- [33] Q. Kong, Y. Xu, I. Sobieraj, W. Wang, and M. D. Plumbley, "Sound event detection and time–frequency segmentation from weakly labelled data," *IEEE/ACM Transactions on Audio, Speech, and Language Processing*, vol. 27, no. 4, pp. 777–787, 2019.
- [34] M. Kachuee, S. Darabi, B. Moatamed, and M. Sarrafzadeh, "Dynamic feature acquisition using denoising autoencoders," *IEEE transactions on neural networks and learning systems*, vol. 30, no. 8, pp. 2252–2262, 2018.
- [35] A. Majumdar, "Blind denoising autoencoder," *IEEE transactions on neural networks and learning systems*, vol. 30, no. 1, pp. 312–317, 2018.
- [36] O. Ronneberger, P. Fischer, and T. Brox, "U-net: Convolutional networks for biomedical image segmentation," in *International Conference on Medical image computing and computer-assisted intervention*. Springer, 2015, pp. 234–241.
- [37] A. Pandey and D. Wang, "A new framework for cnn-based speech enhancement in the time domain," *IEEE/ACM Transactions on Audio, Speech, and Language Processing*, vol. 27, no. 7, pp. 1179–1188, 2019.
- [38] K. Zhang, Y. Li, J. Liang, J. Cao, Y. Zhang, H. Tang, R. Timofte, and L. Van Gool, "Practical blind denoising via swin-conv-unet and data synthesis," *arXiv preprint arXiv:2203.13278*, 2022.
- [39] H. B. Sailor, D. M. Agrawal, and H. A. Patil, "Unsupervised filterbank learning using convolutional restricted boltzmann machine for environmental sound classification," in *Interspeech*, vol. 8, 2017, p. 9.
- [40] W. Ha, C. Singh, F. Lanusse, E. Song, S. Dang, K. He, S. Upadhyayula, and B. Yu, "Adaptive wavelet distillation from neural networks through interpretations," *arXiv preprint arXiv:2107.09145*, 2021.
- [41] S. Xiong, H. Zhou, S. He, L. Zhang, Q. Xia, J. Xuan, and T. Shi, "A novel end-to-end fault diagnosis approach for rolling bearings by integrating wavelet packet transform into convolutional neural network structures," *Sensors*, vol. 20, no. 17, p. 4965, 2020.
- [42] D. Recoskie and R. Mann, "Learning sparse wavelet representations," *arXiv preprint arXiv:1802.02961*, 2018.
- [43] D. Jawali, A. Kumar, and C. S. Seelamantula, "A learning approach for wavelet design," in *ICASSP 2019-2019 IEEE International Conference on Acoustics, Speech and Signal Processing (ICASSP)*. IEEE, 2019, pp. 5018–5022.
- [44] R. R. Coifman, Y. Meyer, and V. Wickerhauser, "Wavelet analysis and signal processing," in *In Wavelets and their applications*. Citeseer, 1992.
- [45] G. Strang and T. Nguyen, *Wavelets and filter banks*. SIAM, 1996.
- [46] S. Mallat, *A wavelet tour of signal processing*. Elsevier, 1999.
- [47] D. P. Kingma and J. Ba, "Adam: A method for stochastic optimization," *arXiv preprint arXiv:1412.6980*, 2014.
- [48] H. Hao, H. Wang, N. ur REHMAN, L. Chen, and H. Tian, "An improved multivariate wavelet denoising method using subspace projection," *IEICE Transactions on Fundamentals of Electronics, Communications and Computer Sciences*, vol. 100, no. 3, pp. 769–775, 2017.
- [49] G. Jimenez-Perez, A. Alcaine, and O. Camara, "U-net architecture for the automatic detection and delineation of the electrocardiogram," in *2019 Computing in Cardiology (CinC)*. IEEE, 2019, pp. Page–1.
- [50] A. Mesaros, T. Heittola, and T. Virtanen, "A multi-device dataset for urban acoustic scene classification," *arXiv preprint arXiv:1807.09840*, 2018.
- [51] E. Fonseca, M. Plakal, F. Font, D. P. Ellis, X. Favory, J. Pons, and X. Serra, "General-purpose tagging of freesound audio with audioset labels: Task description, dataset, and baseline," *arXiv preprint arXiv:1807.09902*, 2018.
- [52] R. R. Coifman and M. V. Wickerhauser, "Entropy-based algorithms for best basis selection," *IEEE Transactions on information theory*, vol. 38, no. 2, pp. 713–718, 1992.